

# Benchmark calculation of $p$ - $^3\text{H}$ and $n$ - $^3\text{He}$ scattering

M. Viviani<sup>a</sup>, A. Deltuva<sup>b</sup>, R. Lazauskas<sup>c</sup>, A. C. Fonseca<sup>d</sup>, A. Kievsky<sup>a</sup>, and L.E. Marcucci<sup>a,f</sup>

<sup>a</sup> *INFN-Pisa, 56127 Pisa, Italy*

<sup>b</sup> *Institute of Theoretical Physics and Astronomy,  
Vilnius University, LT-10222 Vilnius, Lithuania*

<sup>c</sup> *IPHC, IN2P3-CNRS/Université Louis Pasteur BP 28,  
F-67037 Strasbourg Cedex 2, France*

<sup>d</sup> *Centro de Física Nuclear da Universidade de Lisboa,  
P-1649-003 Lisboa, Portugal*

<sup>f</sup> *Department of Physics,  
University of Pisa, 56127 Pisa, Italy*

(Received September 27, 2018)

$p$ - $^3\text{H}$  and  $n$ - $^3\text{He}$  scattering in the energy range above the  $n$ - $^3\text{He}$  but below the  $d$ - $d$  thresholds is studied by solving the 4-nucleon problem with a realistic nucleon-nucleon interaction. Three different methods – Alt, Grassberger and Sandhas, Hyperspherical Harmonics, and Faddeev-Yakubovsky – have been employed and their results for both elastic and charge-exchange processes are compared. We observe a good agreement between the three different methods, thus the obtained results may serve as a benchmark. A comparison with the available experimental data is also reported and discussed.

PACS numbers: 21.45.+v, 21.30.-x, 24.70.+s, 25.10.+s

## I. INTRODUCTION

Modern studies of nuclear structure and dynamics are mostly based on *ab initio* calculations using realistic potentials. Due to the complexity of the problem, it is clearly important to have benchmarks between different groups and different techniques in order to test validity of the existent codes, as well as to establish the numerical accuracy of the solutions. On its turn this may allow a meaningful comparison with experimental data and then serve as a probe on our current understanding of the nuclear dynamics. In particular, this program is well suited to be pursued in few-nucleon systems ( $A \leq 6$ ), where several well controlled numerical techniques have been developed.

The interest in *ab initio* calculations has been renewed in recent years, i.e. after the advent of the theoretical framework of chiral effective field theory ( $\chi\text{EFT}$ ), nowadays widely used to derive nuclear potentials and electroweak currents from the symmetries of QCD—the exact Lorentz, parity, and time-reversal symmetries, and the approximate chiral symmetry (see, for example, Refs. [1–4]). The test of these new potentials in few-nucleon scattering, where accurate measurements of several observables exist, will give very stringent and critical information.

The three-nucleon system is thoroughly studied and for this case some very accurate benchmarks [5, 6] exist. After this achievement focus has been set on the four-nucleon (4N) sector. In first place, this system may serve as an ideal “theoretical laboratory” to test our knowledge of the nucleon–nucleon (NN) and three–nucleon (3N) interactions. In particular, the effects of the NN P-waves and of the 3N force are larger than in the  $A = 2$  or 3 systems, and it is the simplest system where the 3N interaction in channels of total isospin  $T = 3/2$  can be studied. In second place, there is a number of reactions involving four nucleons which are of extreme importance for astrophysics, energy production, and studies of fundamental symmetries. As an example, the reactions  $n + ^3\text{He}$  and  $d + d$  play a key role in the theory of big-bang nucleosynthesis.

Moreover, the potentials derived from  $\chi\text{EFT}$  contain several unknown parameters – the so-called low energy constants (LECs) – which have to be fixed by comparison with experimental data. This fitting procedure is usually brought forth in  $A = 2$  and 3 systems, where accurate calculations can be performed since many years and abundant precise experimental data exist. It is therefore of great interest to test validity of these  $\chi\text{EFT}$  potentials on independent data, which has not been included in the parametrization. The 4N system, containing several resonances which are not straightforwardly correlated with NN and 3N sector, presents an ideal testground.

Nowadays, the 4N bound state problem can be numerically solved with good accuracy. For example, in Ref. [7] the binding energies and other properties of the  $\alpha$ -particle were studied using the AV8' [8] NN interaction; several different techniques produced results in very close agreement with each other (at the level of less than 1%). More recently, the same agreement has also been obtained considering different realistic NN+3N force models [9–12].

In recent years, there has also been a rapid advance in solving the 4N scattering problem with realistic Hamiltonians. Accurate calculations of four-body scattering observables have been achieved in the framework of the Alt-Sandhas-Grassberger (AGS) equations [13], solved in momentum space [14–16], where the long-range Coulomb interaction is treated using the screening and renormalization method [17, 18]. Also solutions of the Faddeev-Yakubovsky (FY) equa-

tions in configuration space [19–23] and the application of the Hyperspherical Harmonics (HH) expansion method [24] to the solution of this problem have been reported [25, 26]. In addition to these methods, the solution of the 4N scattering problem has been obtained also by using techniques based on the resonating group model [27–30]. For applications to  $A > 4$  systems, see Ref. [31] and references therein.

In a previous work, we have presented a benchmark calculation for low energy  $n$ - $^3\text{H}$  and  $p$ - $^3\text{He}$  elastic observables by using the aforementioned AGS, FY, and HH techniques, and by employing different NN interactions [32]. Nice agreement between the results of the three different calculations has been reported, only minor differences were observed for some small polarization observables. It has been concluded that the  $n$ - $^3\text{H}$  and  $p$ - $^3\text{He}$  elastic scattering problem can be nowadays solved with a good accuracy.

In the present paper, we extend the benchmark to  $p$ - $^3\text{H}$  and  $n$ - $^3\text{He}$  scattering for energies where both channels are open but below the  $d-d$  threshold. These calculations present new challenges and are rather complex since the two reaction channels are coupled and involve both total isospin  $T = 0$  and  $T = 1$  states. So far, only a few accurate calculations have been performed for these processes [16, 23]. Only recently, the AGS method has been extended to the energy regime well above breakup threshold where the calculations become even more complicated due to nontrivial boundary conditions or singularities [33]. Therefore, we consider the present benchmark as an important step in establishing our current capability to solve the  $A = 4$  scattering problem. Moreover, our aim is also to provide a set of solid converged results which could represent useful benchmarks for future applications in  $A = 4$  scattering. The potential used in this paper is the N3LO500 model by Entem and Machleidt [34], based on the  $\chi\text{EFT}$  approach and derived up to next-to-next-to-next-to-leading order in chiral perturbation theory.

In addition to the desire of improving theoretical tools, it is important to note that for these reactions there exist a large amount of accurate experimental data, accumulated during the last 50 years. In particular, below the  $d-d$  threshold there exist (since many years) several measurements of the  $p$ - $^3\text{H}$  elastic differential cross section [35–41],  $n$ - $^3\text{He}$  elastic differential cross section [42, 43] and total cross section [42–45], and  $n$ - $^3\text{He}$  elastic analyzing powers [46–50]. Regarding the  $n$ - $^3\text{He} \rightarrow p$ - $^3\text{H}$  charge exchange reaction, there exist mainly measurements of the total cross section [43, 45, 51–57]. For the  $p$ - $^3\text{H} \rightarrow n$ - $^3\text{He}$  charge exchange reactions, there exist measurements of the differential cross section [58–61] and polarization observables [62–66]. Therefore, another motivation of the present work is to compare theoretical predictions with this data.

The paper is organized as follows. In Section II, a brief description of the methods used for this benchmark is reported. In Section III, a comparison between the results obtained within the different schemes is shown and the theoretical calculations are also compared with the available experimental data. The conclusions will be provided in Section IV.

## II. METHODS

In this work three different techniques, namely the AGS equations, the HH method and the FY equations, will be employed to solve 4N scattering problem and the results provided by the three approaches will be benchmarked. Generalities common to the three methods will be discussed in this section, whereas technicalities proper to each technique will be presented separately in devoted sections.

In case of a two body clustering  $A$ - $B$ , the total energy of the scattering state in the center-of-mass (CM) system is given by

$$E = -B_A - B_B + T_{CM} \quad (1)$$

where

$$T_{CM} = \frac{q_\gamma^2}{2\mu_\gamma}, \quad \frac{1}{\mu_\gamma} = \frac{1}{M_A} + \frac{1}{M_B}, \quad (2)$$

$q_\gamma$  is the relative momentum between clusters, and  $M_X$  ( $B_X$ ) is the mass (binding energy) of the cluster  $X$ . Clearly, in the case of a single nucleon  $M_X = M_N$ , where  $M_N$  is the nucleon mass, and  $B_X = 0$ . In this paper, we limit ourselves to study the scattering for  $-B_{^3\text{He}} < E < -2B_d$ , where  $B_d$  is the deuteron binding energy. Namely, we consider 4N scattering when the channels  $p$ - $^3\text{H}$  and  $n$ - $^3\text{He}$  are open, but the  $d$ - $d$  channel is closed.

In the following,  $\gamma$  will denote the particular asymptotic clustering  $A$ - $B$ . More specifically,  $\gamma = 1$  (2) will correspond to the  $p$ - $^3\text{H}$  ( $n$ - $^3\text{He}$ ) asymptotic clustering. Moreover, for example when discussing  $n$ - $^3\text{He}$  scattering, the observables will be calculated at a given neutron laboratory energy  $E_n$ , corresponding approximately to  $E_n \approx (4/3)T_{CM}$ .

For a given total angular momentum quantum number  $J$  and parity  $\pi$ , the information on the scattering observables is contained in the S-matrix  $\mathcal{S}_{\gamma LS, \gamma' L' S'}^{J\pi}$ , where  $\gamma LS$  ( $\gamma' L' S'$ ) denote the initial (final) clustering type, relative orbital momentum and channel spin of the two clusters, respectively (see below). Each submatrix of the S-matrix representing

a separate cluster is clearly no longer unitary. For example, the submatrix describing  $n$ - $^3\text{He}$  elastic scattering will be denoted as  $\mathcal{S}_{\gamma=2 LS, \gamma'=2 L'S'}^{J\pi}(E) \equiv \mathcal{S}_{LS, L'S'}^{n-^3\text{He}, J\pi}(E)$ . For the  $J^\pi = 0^\pm$  channels, submatrix  $\mathcal{S}^{n-^3\text{He}, J\pi}$  is of dimension 1 and can be parametrized in the standard way

$$\mathcal{S}_{LS, LS}^{n-^3\text{He}, J\pi} = \eta_{LS}^{J\pi} \exp(2i\delta_{LS}^{J\pi}). \quad (3)$$

For the other cases,  $\mathcal{S}^{n-^3\text{He}, J\pi}$  is of dimension 2 and is conveniently parametrized as

$$\mathcal{S}^{n-^3\text{He}, J\pi} = \begin{pmatrix} a & b+ic \\ -(b+ic) & a \end{pmatrix}^{-1} \begin{pmatrix} \eta_{LS}^{J\pi} \exp(2i\delta_{LS}^{J\pi}) & 0 \\ 0 & \eta_{L'S'}^{J\pi} \exp(2i\delta_{L'S'}^{J\pi}) \end{pmatrix} \begin{pmatrix} a & b+ic \\ -(b+ic) & a \end{pmatrix}, \quad (4)$$

where the (eigen)phase-shifts  $\delta_{LS}^{J\pi}$ , the (eigen)inelasticity parameters  $\eta_{LS}^{J\pi}$ , and the parameters  $a$ ,  $b$ , and  $c$  are real (and  $a^2 + b^2 + c^2 = 1$ ). Explicitly,  $(a, b+ic)$  and  $(-b-ic, a)$  are the (right) eigenvectors of the matrix  $\mathcal{S}^{n-^3\text{He}, J\pi}$  associated to the two eigenvalues, the latter written as  $\eta_{LS}^{J\pi} \exp(2i\delta_{LS}^{J\pi})$  and  $\eta_{L'S'}^{J\pi} \exp(2i\delta_{L'S'}^{J\pi})$ . Then, we parametrize  $a + i(b+ic) \equiv \exp(i\epsilon^{J\pi})$ . If the matrix  $\mathcal{S}^{n-^3\text{He}, J\pi}$  would be unitary, one recovers the standard definition of mixing parameter  $a = \cos(\epsilon^{J\pi})$ ,  $b = \sin(\epsilon^{J\pi})$ ,  $c = 0$  with  $\epsilon^{J\pi}$  real. On the other hand, with inelastic channels present,  $\epsilon^{J\pi}$  is complex.

### A. AGS Equations

The AGS equations [13] for the four-body transition operators were derived assuming short-range interactions, but together with the screening and renormalization method [15, 17, 18], they can be applied also to systems with repulsive Coulomb force. The isospin formalism enables the symmetrization of the AGS equations [14] in the 4N system, where there are only two distinct four-particle partitions, one of the 3+1 type and one of the 2+2 type, denoted by  $\alpha = 1$  and 2, respectively. In terms of particles 1,2,3,4 we choose those partitions to be (12,3)4 and (12)(34), respectively. The corresponding transition operators  $\mathcal{U}_{\beta\alpha}$  for the initial states of the 3+1 type, as appropriate for the  $n$ - $^3\text{He}$  and  $p$ - $^3\text{H}$  scattering, obey the integral equations

$$\begin{aligned} \mathcal{U}_{11} &= -(G_0 T G_0)^{-1} P_{34} - P_{34} U_1 G_0 T G_0 \mathcal{U}_{11} + U_2 G_0 T G_0 \mathcal{U}_{21}, \\ \mathcal{U}_{21} &= (G_0 T G_0)^{-1} (1 - P_{34}) + (1 - P_{34}) U_1 G_0 T G_0 \mathcal{U}_{11}. \end{aligned} \quad (5)$$

Here  $G_0 = (E + i0 - H_0)^{-1}$  is the free resolvent,  $H_0$  is the free Hamiltonian,  $P_{ij}$  is the permutation operator of particles  $i$  and  $j$ ,  $T = V + V G_0 T$  is the two-nucleon transition matrix derived from the potential  $V$ , and

$$U_\alpha = P_\alpha G_0^{-1} + P_\alpha T G_0 U_\alpha, \quad (7)$$

are 3+1 and 2+2 subsystem transition operators with  $P_1 = P_{12} P_{23} + P_{13} P_{23}$  and  $P_2 = P_{13} P_{24}$ .

The integral AGS equations (5) are solved in momentum-space partial-wave framework. Scattering amplitudes for elastic and charge-exchange reactions are given by on-shell matrix elements of  $\mathcal{U}_{11}$  as described in Refs. [14, 16, 33] where also further details regarding the numerical solution can be found. Note that in the considered energy regime the only singularities in the kernel of AGS equations arise due to bound-state poles of  $U_1$  and are treated by a simple subtraction method.

### B. HH Expansion

The wave function describing a scattering process with incoming clusters specified by the index  $\gamma$  and in a state of total angular momentum quantum numbers  $J, J_z$ , relative orbital angular momentum  $L$ , and channel spin  $S$  ( $S = 0, 1$ ) can be written as

$$\Psi_{1+3}^{\gamma LS, JJ_z} = \Psi_C^{\gamma LS, JJ_z} + \Psi_A^{\gamma LS, JJ_z}, \quad (8)$$

keeping in mind the notation  $\gamma = 1$  (2) to represent respectively  $p$ - $^3\text{H}$  ( $n$ - $^3\text{He}$ ) asymptotic clustering.

The ‘‘core’’ part of wave function  $\Psi_C^{\gamma LS, JJ_z}$  describes the system in the region where four particles are close to each other and where their mutual interactions are strong. Hence,  $\Psi_C^{\gamma LS, JJ_z}$  vanishes in the limit of large inter-cluster distances. This part of the wave function is written as a linear expansion  $\sum_\mu c_\mu^{\gamma LSJ} \mathcal{Y}_\mu$ , where  $\mathcal{Y}_\mu$  is a set of basis functions constructed in terms of the HH functions (for more details see, for example, Ref. [24]).

The other part  $\Psi_A^{\gamma LS, JJ_z}$  describes the relative motion of the clusters in the asymptotic regions, where these clusters do not interact (except eventually for the long-range Coulomb interaction). In the asymptotic region the wave function  $\Psi_{1+3}^{\gamma LS, JJ_z}$  reduces to  $\Psi_A^{\gamma LS, JJ_z}$ , which must therefore be the appropriate asymptotic solution of the Schrödinger equation. Then,  $\Psi_A^{\gamma LS, JJ_z}$  can be decomposed into a linear combination of the following functions

$$\begin{aligned} \Omega_{\gamma LS}^{\pm} &= \mathcal{A} \left\{ \left[ Y_L(\hat{\mathbf{y}}_\gamma) \otimes [\phi_A \otimes \phi_B]_S \right]_{JJ_z} \right. \\ &\quad \left. \times \left( f_L(y_l) \frac{G_L(\eta_\gamma, q_\gamma y_\gamma)}{q_\gamma y_\gamma} \pm i \frac{F_L(\eta_\gamma, q_\gamma y_\gamma)}{q_\gamma y_\gamma} \right) \right\}, \end{aligned} \quad (9)$$

where  $y_\gamma$  is the distance between the CM of clusters  $A$  and  $B$ ,  $q_\gamma$  is the magnitude of the relative momentum between the two clusters (see Eq. (2)), and  $\phi_A$  and  $\phi_B$  the corresponding bound state wave functions. In the present work, the trinucleon bound state wave functions are calculated very accurately by means of the HH method [10, 24] using the corresponding  $A = 3$  Hamiltonian. Conventionally, we identify the trinucleon bound state wave function with  $\phi_A$ . Therefore,  $\phi_B$  describes the single nucleon spin-isospin state. The channel spin  $S$  is obtained by coupling the angular momentum of the two clusters. In our case, clearly  $S = 0, 1$ . The symbol  $\mathcal{A}$  means that the expression between the curly braces has to be properly antisymmetrized.

In Eq. (9), the functions  $F_L$  and  $G_L$  describe the asymptotic radial motion of the clusters  $A$  and  $B$ . If the two clusters are composed of  $Z_A$  and  $Z_B$  protons, respectively, the parameter  $\eta_\gamma = \mu_\gamma Z_A Z_B e^2 / q_\gamma$ , where  $e^2 \approx 1.44$  MeV fm. The function  $F_L(\eta, qy)$  is the regular Coulomb function while  $G_L(\eta, qy)$  is the irregular Coulomb function. The function  $f_L(y) = [1 - \exp(-\beta y)]^{2L+1}$  in Eq. (9) has been introduced to regularize  $G_L$  at small  $y$ , and  $f_L(y) \rightarrow 1$  as  $y$  is large, thus not affecting the asymptotic behavior of  $\Psi_{1+3}^{\gamma LS, JJ_z}$ . Note that for large values of  $qy_l$ ,

$$\begin{aligned} f_L(y_l) G_L(\eta, qy_l) \pm i F_L(\eta, qy_l) &\rightarrow \\ \exp \left[ \pm i (qy_l - L\pi/2 - \eta \ln(2qy_l) + \sigma_L) \right], \end{aligned} \quad (10)$$

where  $\sigma_L$  is the Coulomb phase-shift. If  $\eta$  is zero, the Coulomb functions reduce to the Riccati-Bessel functions [67]. Therefore,  $\Omega_{\gamma LS, JJ_z}^+$  ( $\Omega_{\gamma LS, JJ_z}^-$ ) describe the asymptotic outgoing (incoming)  $A - B$  relative motion. Finally,  $\Psi_A^{\gamma LS, JJ_z}$  is given by

$$\Psi_A^{\gamma LS, JJ_z} = \Omega_{\gamma LS, JJ_z}^- - \sum_{\gamma' L' S'} \mathcal{S}_{\gamma LS, \gamma' L' S'}^{J\pi}(E) \Omega_{\gamma' L' S', JJ_z}^+, \quad (11)$$

where the parameters  $\mathcal{S}_{\gamma LS, \gamma' L' S'}^{J\pi}(E)$  are the  $S$ -matrix elements at the energy  $E$ , given by Eq. (1). Of course, the sum over  $L'$  and  $S'$  is over all values compatible with the given  $J$  and parity  $\pi$ . In particular, the sum over  $L'$  is limited to include either even or odd values such that  $(-1)^{L'} = (-1)^L = \pi$ . The sum over  $\gamma'$  is limited to the *open* channels (namely those channels for which  $q_\gamma^2 > 0$ , see Eq. (2)). For the scattering process considered in the present paper, clearly  $\gamma' = 1, 2$ .

The  $S$ -matrix elements  $\mathcal{S}_{\gamma LS, \gamma' L' S'}^{J\pi}(E)$  and coefficients  $c_\mu^{\gamma LSJ}$  occurring in the HH expansion of  $\Psi_C^{\gamma LS, JJ_z}$  are determined by forming a functional

$$[\mathcal{S}_{\gamma LS, \gamma' L' S'}^{J\pi}(E)] = \mathcal{S}_{\gamma LS, \gamma' L' S'}^{J\pi}(E) - \frac{1}{2i} \left\langle \Psi_{1+3}^{\gamma' L' S', JJ_z} | H - E | \Psi_{1+3}^{\gamma LS, JJ_z} \right\rangle \quad (12)$$

stationary with respect to variations in  $\mathcal{S}_{\gamma LS, \gamma' L' S'}^{J\pi}$  and  $c_\mu^{\gamma LSJ}$  (Kohn variational principle). By applying this principle, a linear set of equations is obtained for  $\mathcal{S}_{\gamma LS, \gamma' L' S'}^{J\pi}$  and  $c_\mu^{\gamma LSJ}$ . This linear system is solved using the Lanczos algorithm.

This method can be applied in either coordinate or momentum space, and using either local or non-local potentials [24]. The first steps are (1) the use of the method discussed in Ref. [68] to antisymmetrize the HH functions and (2) a partial wave decomposition of the asymptotic functions  $\Omega_{\gamma LS, JJ_z}^{\pm}$ , the latter task being rather time consuming. After this decomposition, the calculation of the matrix element in Eq. (12) is fast, except for the  $J^\pi = 2^-$  state, due to the large number of HH functions to be included in the expansion in this particular case. After these steps, the problem reduces to the solution of a linear system.

The expansion of the scattering wave function in terms of the HH basis is in principle infinite, therefore a truncation scheme is necessary. The HH functions are essentially characterized by the orbital angular momentum quantum numbers  $\ell_i$ ,  $i = 1, 3$ , associated with the three Jacobi vectors, and the grand angular quantum number  $K$  (each HH function is a polynomial of degree  $K$ ). The basis is truncated to include states with  $\ell_1 + \ell_2 + \ell_3 \leq \ell_{\max}$  (with all possible re-coupling between angular and spin states appropriate to the given  $J$ ). Between these states, we retain

$\ell_{\max}$	$\eta_{11}^{0-}$	$\delta_{11}^{0-}$ (deg)
1	0.603	+21.9
3	0.459	- 9.9
5	0.505	-10.5
AGS	0.553	-10.5

TABLE I:  $n$ - $^3\text{He}$  inelasticity parameter  $\eta_{11}^{0-}$  and phase-shift  $\delta_{11}^{0-}$  the  $J^\pi = 0^-$  wave at  $E_n = 1.0$  MeV, obtained with the HH method as a function of  $\ell_{\max}$  (see the text for details). The calculations have been performed using the the N3LO500 potential.

only the HH functions with  $K \leq K_{\max}$ . Note that in the calculation we have included both states with total isospin  $T = 0$  and 1.

The main sources of numerical uncertainties for this method could come from the numerical integration needed to compute the matrix elements of the Hamiltonian and the truncation of the basis. It has been checked that the numerical uncertainty of the calculated phase-shifts related to the numerical integration is small (around 0.1 %). The NN interaction has been limited to act on two-body states with total angular momentum  $j \leq j_{\max} = 8$  (greater values of  $j_{\max}$  are completely negligible). The largest uncertainty is related to the use of a finite basis due to the slow convergence of the results with  $K_{\max}$ . This problem can be partially overcome by performing calculations for increasing values of  $K_{\max}$  and then using some extrapolation rule (see for example Ref. [69]) to get the “ $K_{\max} \rightarrow \infty$ ” result. This procedure introduces a new uncertainty which can be estimated. A detailed study of this problem will be published elsewhere [70]. The convergence of the quantities of interest in term of  $K_{\max}$  is slower using NN potentials with a strong repulsion at short interparticle distance, but it is less relevant for the N3LO500 potential. For the present case, this uncertainty has been estimated to be at most 0.5 %.

The convergence with  $\ell_{\max}$  is usually rather fast and values of  $\ell_{\max}$  around either 5 or 6 have been found to be sufficient. However, in some cases, we have found a slow convergence of the inelasticity parameters  $\eta_{LS}^{J^\pi}$ . To give an example, in Table I, we report the values of the  $n$ - $^3\text{He}$   $\eta_{LS}^{J^\pi}$  and  $\delta_{LS}^{J^\pi}$  parameters for the  $J^\pi = 0^-$  wave, calculated with the HH method as a function of  $\ell_{\max}$ . The calculations have been performed at  $E_n = 1$  MeV and for the N3LO500 potential. For this wave the parity is negative, so only HH functions having  $\ell_{\max}$  odd have to be included in the expansion. As can be seen, the inclusion in the expansion of the “core” part of functions with  $\ell_{\max} = 1$  is insufficient to obtain a reasonable estimate of these parameters. The addition of also the  $\ell_{\max} = 3$  functions improves noticeably the calculation of the phase-shift  $\delta_{11}^{0-}$ , which is now very close to the final result (in the table, we have also reported the same parameters obtained using the AGS equations). The inclusion of the  $\ell_{\max} = 5$  brings finally the HH results in agreement with that obtained by the AGS method. On the other hand, the  $\eta_{11}^{0-}$  values appears to converge slowly. Note that for  $p$ - $^3\text{He}$  scattering (see our previous benchmark [32]) only one asymptotic channel is open, so in all calculations one obtains  $\eta_{11}^{0-} = 1$  with a very good accuracy.

### C. Faddeev-Yakubovsky equations in configuration space

In late sixties Yakubovsky [71, 72] generalized a set of equations proposed by Faddeev [71], to treat scattering problems beyond  $A = 3$  case. Based on the arithmetic properties, which arise from the subsequent breaking of  $N$ -particle system into its sub-clusters, FY formalism offers a natural way to decompose system’s wave function into the so called Faddeev-Yakubovsky’s components (FYC). As a result FYC represent the natural structures to impose a proper wave function behavior at the boundaries. A four-particle system requires to introduce FYC of two distinct types: components  $K$  and  $H$ . Asymptotes of components  $K$  incorporate 3+1 particle channels, while components  $H$  contain asymptotes of 2+2 particle channels (see Fig.1). By interchanging order of particles one can construct twelve different components of the type  $K$  and six of the type  $H$ . The system wave function is then represented simply as a sum of these 18 FYC.

Employing the formalism of isospin, protons and neutrons become two distinct states of the same particle (nucleon). For a system of four identical particles there exist only two independent FYC, one of type  $K$  and one of type  $H$ . The other 16 FYC can be obtained from the two independent FYC by applying particle permutation operators (*i.e.* interchanging the order of particles in the system). Similarly only two independent FY equations exist; by singling out  $K \equiv K_{1,23}^4$  and  $H \equiv H_{12}^{34}$ , the set of two FY equations read [20, 22]:

$$\begin{aligned}
 (E - H_0 - V_{12}) K &= V_{12}(P^+ + P^-) [(1 + Q)K + H], \\
 (E - H_0 - V_{12}) H &= V_{12}\tilde{P} [(1 + Q)K + H].
 \end{aligned}
 \tag{13}$$

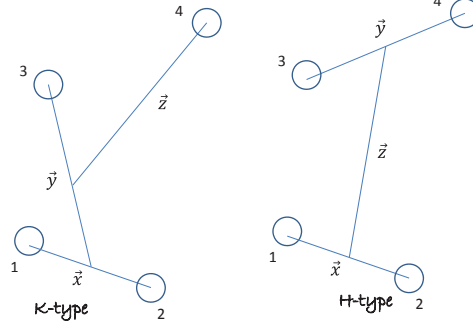


FIG. 1: FY's components  $K$  and  $H$ . Asymptotically as  $z \rightarrow \infty$  components  $K$  describe 3+1 particle channels, whereas components  $H$  contains asymptotic states of 2+2 channels.

The particle permutation operators  $P^+$ ,  $P^-$ ,  $\tilde{P}$  and  $Q$  represent simply different combinations of two-particle transposition operators:

$$\begin{aligned} P^+ &= (P^-)^{-1} = P_{23}P_{12} , \\ Q &= -P_{34} , \\ \tilde{P} &= P_{13}P_{24} = P_{24}P_{13} . \end{aligned}$$

Employing the operators defined above, the wave function of the system is given by

$$\Psi = [1 + (1 + P^+ + P^-)Q] (1 + P^+ + P^-)K + (1 + P^+ + P^-)(1 + \tilde{P})H. \quad (14)$$

The functions  $K$  and  $H$  are expanded in the basis of partial angular momentum, spin and isospin variables, according to:

$$\Phi_i(\vec{x}_i, \vec{y}_i, \vec{z}_i) = \sum_{\alpha} \frac{\mathcal{F}_i^{\alpha}(x_i, y_i, z_i)}{x_i y_i z_i} Y_i^{\alpha}(\hat{x}_i, \hat{y}_i, \hat{z}_i) , \quad (15)$$

where the functions  $Y_i^{\alpha}(\hat{x}_i, \hat{y}_i, \hat{z}_i)$  are defined below. The Jacobi coordinates, associated with each type of FYC  $K$  and  $H$ , are used to represent our wave functions (see Fig. 1). Such a choice of coordinates permits us to separate the center of mass motion and guarantees that the kinetic energy operator is independent of angular variables. The angular dependence is hidden in tripolar harmonics  $Y_i^{\alpha}(\hat{x}_i, \hat{y}_i, \hat{z}_i)$ , which in addition to angular momentum variables comprise spins and isospins of the nucleons. To couple the angular and spin quantum numbers, a slightly different scheme is employed compared to AGS and HH methods, namely the  $jj$ -coupling scheme, which is defined by:

$$\left[ \left\{ (t_i t_j)_{t_x} t_k \right\}_{T_3} t_l \right]_{TT_z} \left\langle \left\{ \left[ l_x (s_i s_j)_{\sigma_x} \right]_{j_x} \left[ l_y (s_k)_{j_y} \right]_{J_3} \left[ l_z (s_l)_{j_z} \right]_{J^{\pi} J_z} \right\} \right\rangle \quad (16)$$

for the components of  $K$ -type, and

$$\left[ (t_i t_j)_{t_x} (t_k t_l)_{t_y} \right]_{TT_z} \left\langle \left\{ \left[ l_x (s_i s_j)_{\sigma_x} \right]_{j_x} \left[ l_y (s_k s_l)_{\sigma_y} \right]_{j_{xy}} \right\} l_z \right\rangle_{J^{\pi} J_z} \quad (17)$$

for the  $H$ -type components. Here  $s_i = 1/2$  and  $t_i = 1/2$  are the spin and isospin quantum numbers of the individual nucleons and  $(J^{\pi}, T)$  are, respectively, the total angular momentum, parity and isospin of a four-body system. By  $J_z$  and  $T_z$  we identify the projection of the system total angular momentum and isospin on the selected axis. Nuclear Hamiltonian conserves the system parity and angular momentum  $J^{\pi}$ ; the system wave function is also invariant for the rotations around the fixed axis (so one can also fix projection quantum number  $J_z$ ). Furthermore the system made of two protons and two neutrons has  $T_z \equiv 0$ . Then each amplitude  $\mathcal{F}_i^{\alpha}(x_i, y_i, z_i)$  is labeled by a set of 11 non-fixed quantum numbers  $\alpha$ . On contrary a total isospin  $T$  of the system is not conserved, it is allowed to take values  $T = 0, 1$  and 2. Combination of different total isospin channels is necessary in order to separate unambiguously the  $p$ - $^3\text{H}$  and  $n$ - $^3\text{He}$  channels [20].

By projecting each of Eqs. (13) on its natural configuration space basis, one obtains a system of coupled integro-differential equations. To keep the number of these equations finite, one is obliged to introduce some additional

truncations in the partial wave expansion given in Eq. (15), by considering only the most relevant amplitudes. This truncation is realized by imposing the condition  $\max(l_x, l_y, l_z) \leq 4$  on the maximal partial angular momenta.

Equations (13) are not complete as long as they are not complemented with the appropriate boundary conditions. First, FY amplitudes, for bound as well as for scattering states, satisfy the regularity conditions:

$$\mathcal{F}_i^\alpha(0, y_i, z_i) = \mathcal{F}_i^\alpha(x_i, 0, z_i) = \mathcal{F}_i^\alpha(x_i, y_i, 0) = 0. \quad (18)$$

The proper asymptotic behavior of the FY components of type- $K$  for the scattering process is implemented in a similar way as for the HH method, see Eq. (8), i.e., by splitting the FY amplitude into two terms: a square integrable core-term  $\mathcal{F}_{C,i}^\alpha(x_i, y_i, z_i)$  and a long-ranged term  $\mathcal{F}_{A,i}^\alpha(x_i, y_i, z_i)$ , which describes the behavior of FY amplitudes in the far asymptotic regions,

$$\mathcal{F}_i^\alpha(x_i, y_i, z_i) = \mathcal{F}_{C,i}^\alpha(x_i, y_i, z_i) + \mathcal{F}_{A,i}^\alpha(x_i, y_i, z_i). \quad (19)$$

As explained in the previous section, the asymptotic part  $\mathcal{F}_{A,i}^\alpha(x_i, y_i, z_i)$  is constructed from the calculated three-nucleon wave functions (either  ${}^3\text{H}$  or  ${}^3\text{He}$  nucleus) and involves a few parameters associated with a scattering matrix to be determined, see Eq. (11). This term is treated as an inhomogeneous one when solving numerically the FY equations. The core part of the FY partial amplitudes is expanded on the basis of Lagrange-Laguerre mesh functions, employing Lagrange-mesh method [73]:

$$\mathcal{F}_{C,i}^\alpha(x_i, y_i, z_i) = C^{\alpha,k,l,m} f_k^x(x_i) f_l^y(y_i) f_m^z(z_i)$$

with  $C^{\alpha,k,l,m}$  representing some unknown coefficients, while the  $f_k^x(x_i)$ ,  $f_l^y(y_i)$  and  $f_m^z(z_i)$  are Lagrange-Laguerre basis functions associated with each radial variable. The set of integro-differential equations is transformed into a linear algebra problem by projecting these equations on a chosen three-dimensional Lagrange-Laguerre basis. The coefficients  $C^{\alpha,k,l,m}$  are determined by solving the resulting linear algebra problem and by applying Kohn-variational principle to determine the scattering matrix associated with the inhomogeneous terms of Eq. (19).

### III. RESULTS

In this section the results obtained using the three different methods are compared between themselves as well as with available experimental data for some selected observables. First, in Tables II and III we present the  $n$ - ${}^3\text{He}$  phase-shifts and inelasticity parameters for the most relevant waves calculated using the three different methods. Calculations have been carried out for three different neutron laboratory energies,  $E_n = 1, 2,$  and  $3.5$  MeV, corresponding to cases where experimental data exist. In particular, we compare the parameters computed by the three methods for the states  $J^\pi = 0^\pm, 1^\pm,$  and  $2^-$ . The scattering in other  $J^\pi$  states is dominated by the centrifugal barrier and therefore their  $S$ -matrices only slightly deviates from the unity matrix, while the results are not very sensitive to the interaction and the method used to calculate them. Note that the calculations of the observables has been performed including states up to  $J = 4$ . In all the cases, the wave function contains states of total isospin  $T = 0$  and  $1$ .

Clearly the values of these parameters may depend on the adopted choice of the coupling scheme between the spin of the two clusters and the spherical harmonic function  $Y_L(\mathbf{y})$  in the asymptotic functions  $\Omega_{LS}^\pm$  (see Eq.(9)). As specified in the previous section, each group has chosen a different coupling scheme. It can be shown, however, that the (eigen)phase-shifts defined as discussed above are coupling scheme-independent, on contrary, the mixing parameter depends on coupling scheme (however, they are related to each other by some constant factor). In the following we have decided to report the mixing parameters which are proper to the coupling scheme specified in Eq. (9).

In Tables II and III we present the inelasticity parameters, phase-shifts, and mixing parameters for  $n$ - ${}^3\text{He}$  scattering obtained using the N3LO500 potential at the selected energies. By inspecting the tables, we can notice a reasonable agreement between the results obtained by the three different techniques.

As presented in Table II, for  $0^\pm$  waves we note a large deviation of the inelasticity parameters from unity. In these waves, a  $n$ - ${}^3\text{He}$  initial state will mostly end up in a  $p$ - ${}^3\text{H}$  final state (and vice versa). The phase-shifts are in very good agreement, only in a few cases the results differ by more than 1%. Larger differences are found for the inelasticity parameters (up to 10%), related with the aforementioned slow convergence for these values within the HH method. Note that the  $n$ - ${}^3\text{He}$   $0^-$  phase-shifts are negative, meaning that the effective interaction between the two clusters is mostly repulsive in this wave. This is at variance with the  $p$ - ${}^3\text{He}$  scattering case, where it was found that the interaction is attractive for the same wave. Inelasticity parameter for  $1^+$  wave is found to be close to unity. For this wave, the Pauli repulsion keeps the incident clusters well apart, preventing particle recombination process.

Let us now inspect Table III. For the  $1^-$  state, it is possible to note that the  $LS = 10$  ( ${}^1P_1$ ) phase-shift is negative showing that the interaction of the  $n$ - ${}^3\text{He}$  clusters is repulsive (again, for this wave the  $p$ - ${}^3\text{He}$  phase-shift is positive).

$E_n$ (MeV)	$\eta^{0+}$	$\delta^{0+}$ (deg)	$\eta^{0-}$	$\delta^{0-}$ (deg)	$\eta_{01}^{1+}$	$\delta_{01}^{1+}$ (deg)	$\eta_{21}^{1+}$	$\delta_{21}^{1+}$ (deg)	$\Re(\epsilon^{1+})$ (deg)	$\Im(\epsilon^{1+})$ (deg)	Method
1.0	0.267	-63.4	0.553	-10.5	0.998	-31.8	1.000	-0.054	0.306	0.001	AGS
	0.267	-63.2	0.545	-10.4	0.997	-31.8	1.000	-0.058	0.228	0.001	FY
	0.259	-64.0	0.505	-10.5	0.998	-32.4	1.000	-0.065	0.297	0.001	HH
2.0	0.162	-81.4	0.380	-12.9	0.997	-43.8	1.000	-0.220	0.585	0.003	AGS
	0.162	-81.4	0.368	-12.7	0.997	-43.8	1.000	-0.184	0.467	0.006	FY
	0.147	-82.2	0.348	-12.9	0.996	-44.3	1.000	-0.250	0.574	0.002	HH
3.5	0.086	-97.6	0.093	-8.48	0.996	-56.0	1.000	-0.567	0.971	0.007	AGS
	0.086	-98.2	0.075	-8.41	0.996	-56.3	1.000	-0.566	0.884	0.003	FY
	0.074	-98.5	0.088	-8.16	0.996	-56.2	1.000	-0.618	0.957	0.004	HH

TABLE II:  $n$ - $^3\text{He}$  inelasticity parameters  $\eta_{LS}^{J\pi}$ , phase-shifts  $\delta_{LS}^{J\pi}$ , and mixing parameters  $\epsilon^{J\pi}$  for the  $J^\pi = 0^\pm$  and  $1^+$  waves at  $E_n = 1.0, 2.0,$  and  $3.5$  MeV, obtained with the three methods described in the text. The phase-shifts and mixing parameters are given in degrees. The calculations have been performed using the N3LO500 potential.

$E_n$ (MeV)	$\eta_{10}^{1-}$	$\delta_{10}^{1-}$ (deg)	$\eta_{11}^{1-}$	$\delta_{11}^{0-}$ (deg)	$\Re(\epsilon^{1-})$ (deg)	$\Im(\epsilon^{1-})$ (deg)	$\eta_{11}^{2-}$	$\delta_{11}^{2-}$ (deg)	$\eta_{31}^{2-}$	$\delta_{31}^{2-}$ (deg)	$\Re(\epsilon^{2-})$ (deg)	$\Im(\epsilon^{2-})$ (deg)	Method
1.0	0.959	-0.263	0.994	7.43	-1.98	-0.869	0.923	17.5	1.000	0.003	-0.249	-0.093	AGS
	0.958	-0.333	0.995	7.57	-2.02	-0.849	0.938	17.3	1.000	0.002	-0.208	-0.092	FY
	0.957	-0.295	0.993	7.57	-2.02	-0.909	0.938	17.0	1.000	0.003	-0.248	-0.086	HH
2.0	0.864	-0.806	0.985	20.0	-1.96	-1.32	0.665	47.1	1.000	0.021	-0.330	-0.286	AGS
	0.862	-0.750	0.986	20.2	-1.96	-1.36	0.685	47.0	1.000	0.012	-0.301	-0.248	FY
	0.859	-0.865	0.989	20.5	-1.94	-1.37	0.715	47.0	1.000	0.022	-0.334	-0.283	HH
3.5	0.699	-2.60	0.992	38.6	-1.90	-1.65	0.676	70.8	1.000	0.101	-0.237	-0.422	AGS
	0.694	-2.65	0.990	38.1	-1.87	-1.75	0.681	70.4	1.000	0.078	-0.255	-0.415	FY
	0.694	-2.56	0.994	37.3	-1.87	-1.75	0.714	69.1	1.000	0.092	-0.259	-0.408	HH

TABLE III: Same as for Table but for the  $J^\pi = 1^-$  and  $2^-$  waves.

In this case, the inelasticity parameter deviates sizably from unity. On the other hand, the  $LS = 11$  ( $^3P_1$ ) phase-shift is positive and large as for  $p$ - $^3\text{He}$ , while  $\eta_{11}^{1-} \approx 1$ . We note a good agreement between the results obtained by the three different methods for these parameters, and also for the mixing parameter  $\epsilon^{1-}$ . For the  $2^-$  state, the  $LS = 11$  ( $^3P_2$ ) phase-shift is positive and large as for  $p$ - $^3\text{He}$ , while the corresponding inelasticity parameter decreases at low energies and then reaches a sort of plateau between  $E_n = 2$  and  $3.5$  MeV. There is a good agreement for the phase-shifts, while for the inelasticity parameters we observe again a somewhat sizable deviation between the results obtained with the HH and the AGS/FY methods, again connected to the slow convergence of the HH expansion. The  $LS = 31$  ( $^3F_2$ ) phase-shift  $\delta_{31}^{2-}$  and mixing parameter  $\epsilon^{2-}$  are rather small, due to the large centrifugal barrier (in this case  $\eta_{31}^{2-}$  is very close to 1). In any case, we observe a reasonable agreement between different calculation methods even for these tiny quantities.

Let us now examine how the good agreement found for the phase-shifts and mixing parameters calculated with the three different methods is reflected in the experimental observables. Let us start with a case of  $n$ - $^3\text{He}$  elastic observables. We have considered the differential cross section, the neutron analyzing power  $A_{y0}$ , the  $^3\text{He}$  analyzing power  $A_{0y}$ , and the spin correlation coefficient  $A_{yy}$ . The analyzing power observables are rather sensitive to small variations of the P-wave phase-shifts in the kinematical regime considered in this paper, while  $A_{yy}$  is also sensitive to the S-wave phase shifts.

In Figs. 2, 3, and 4 we have reported the results obtained using the AGS equation (blue solid lines), the HH expansion method (green dashed lines), and the FY equations (red dot-dash lines) using the N3LO500 potential for  $E_n = 1, 2,$  and  $3.5$  MeV, respectively. Where available, we compare the calculated observables with the experimental data. As can be seen by inspecting the three figures, for the differential cross section the three curves almost always perfectly coincide and can be hardly distinguished. For the  $A_{y0}$  and  $A_{0y}$  analyzing power observables, the AGS and FY results almost coincide, while the HH results slightly differ (however, we note that the differences between the three calculations are in any case within the experimental error-bars). We also note in Fig. 2 a rather strong

energy-dependence of the analyzing power from the measurements at  $E_n = 0.944, 1, \text{ and } 1.053 \text{ MeV}$  [49]. For the  $A_{yy}$  observable, the predictions obtained by the three methods are slightly at variance. This observable, as already stated, is quite sensitive to the  $0^+$  phase shift, for which the convergence of the three methods is more problematic. In spite of these difficulties, the agreement in the considered observable is still acceptable.

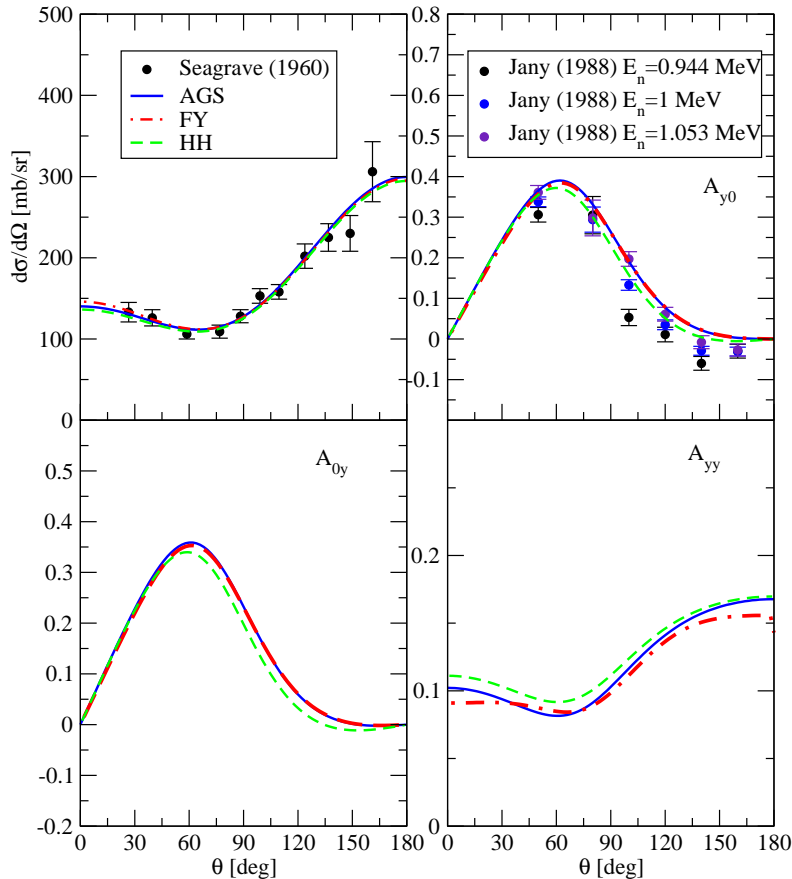


FIG. 2: (Color online) Differential cross section, proton analyzing power  $A_{y0}$ ,  ${}^3\text{He}$  analyzing power  $A_{0y}$ , and spin correlation coefficient  $A_{yy}$  for  $n$ - ${}^3\text{He}$  elastic scattering at  $E_n = 1 \text{ MeV}$  neutron lab energy obtained using the N3LO500 potential. The lines show the results obtained using the AGS (blue solid lines), FY (red dot-dash lines), and the HH (green dashed lines) methods. The experimental data are from Refs. [42, 49].

Let us now consider the  $p$ - ${}^3\text{H}$  elastic observables. For this case, we have decided to show the comparison of the theoretical results for the differential cross section and the proton analyzing power  $A_{y0}$ , where experimental data are available. These observables are reported in Fig. 5 for three different energies of the proton beam,  $E_p = 2.5, 3.5 \text{ and } 4.15 \text{ MeV}$ . In the upper panels, we have reported the differential cross sections and in the lower panels the proton analyzing power  $A_{y0}$ . As it can be seen, the AGS and FY results are almost indistinguishable for all the considered cases. The HH results show somewhere a slight deviation from the AGS/FY values, probably due to the slow convergence observed for the inelasticity parameters.

Regarding the comparison with the experimental data, we note again a good reproduction of the differential cross sections at all the energies. For  $A_{y0}$  at  $E_p = 4.15 \text{ MeV}$ , the only case for which there are experimental data for this observable, we note a slight underprediction of the peak and at forward angles, where the nuclear and Coulomb scattering amplitudes interfere.

In Fig. 6, the comparison is extended to the reaction  $p$ - ${}^3\text{H} \rightarrow n$ - ${}^3\text{He}$ . Also in this case, we have reported the differential cross section and proton analyzing power at  $E_p = 2.5, 3.5 \text{ and } 4.15 \text{ MeV}$ . The  $p$ - ${}^3\text{H} \rightarrow n$ - ${}^3\text{He}$  differential cross section has been found to depend strongly on the  $2^-$  wave, and it is therefore rather sensitive to the convergence of the calculations. For this reason, we observe more sizeable deviations between the AGS/FY and HH results. In any case, from panels (b) and (c), it is possible to note a clear discrepancy among the theoretical calculations and the experimental data at backward angles. Regarding  $A_{y0}$ , we observe a fair agreement between the theoretical results. Here, we note an overprediction of the calculated  $A_{y0}$  in the maximum region with respect to the available

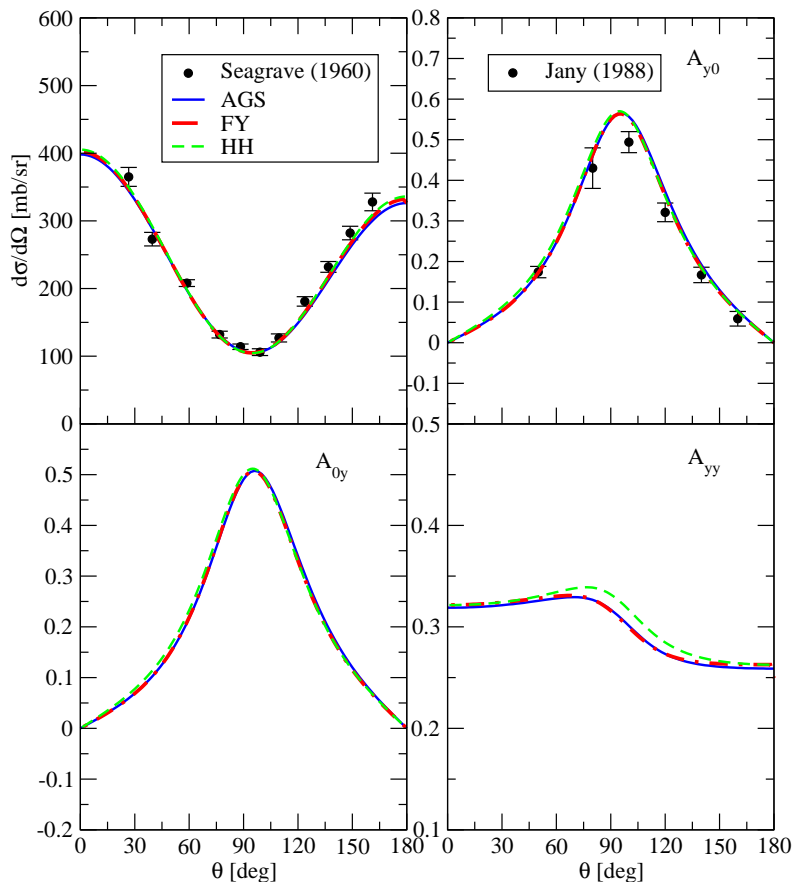


FIG. 3: (Color online) Same as Fig. 2 but for neutron energy  $E_n = 2$  MeV. The experimental data are from Refs. [42, 49].

experimental data. At  $E_p = 3.5$  MeV, see panel (e), theoretical calculations and data also disagree in the region of the minimum. The origin of these discrepancies is still not clear. Moreover, we note that in Ref. [16], using four realistic NN potentials, a significant sensitivity of charge-exchange observables to the NN force model has been found.

#### IV. CONCLUSIONS

In this work, we have studied some low energy  $n$ - $^3\text{He}$  and  $p$ - $^3\text{H}$  elastic and charge-exchange observables by using three different approaches, the HH, AGS and FY techniques. Very accurate solutions of the 4N scattering problem using the AGS technique [14–16] were obtained already a few years ago. The long-range Coulomb interaction in this approach is taken into account using the screening and renormalization method [17, 18]. In recent years, after adding some additional numerical power, also the accuracy of the calculations performed using the HH and FY techniques increased [23, 25, 26]. Therefore, it becomes quite interesting to compare the results obtained by the different methods in order to test their capability to solve the 4N scattering problem. Around five years ago, some of the authors of the present paper presented a very detailed comparison for  $p$ - $^3\text{He}$  and  $n$ - $^3\text{H}$  observables [32]. The aim of the present paper is to extend the benchmark to the  $n$ - $^3\text{He}$  and  $p$ - $^3\text{H}$  scattering.

Here we have shown that for N3LO500 potential the results obtained by the different techniques are in good agreement. In particular, FY and AGS results are in a very good agreement. The phase-shifts, mixing angles and observables calculated using the HH method show some small deviations from those obtained by AGS/FY techniques. Anyway, the differences are tiny, and usually do not exceed the experimental errors. Therefore, we can conclude that all the considered theoretical methods have reached a rather high level of accuracy in the description of  $n$ - $^3\text{He}$  and  $p$ - $^3\text{H}$  elastic and charge-exchange scattering making comparison with experiment reliable and meaningful.

Concerning the comparison with the experiments, in most of the cases we have observed a good agreement between the results obtained using the N3LO500 potential and the available experimental data. Some disagreements persist for

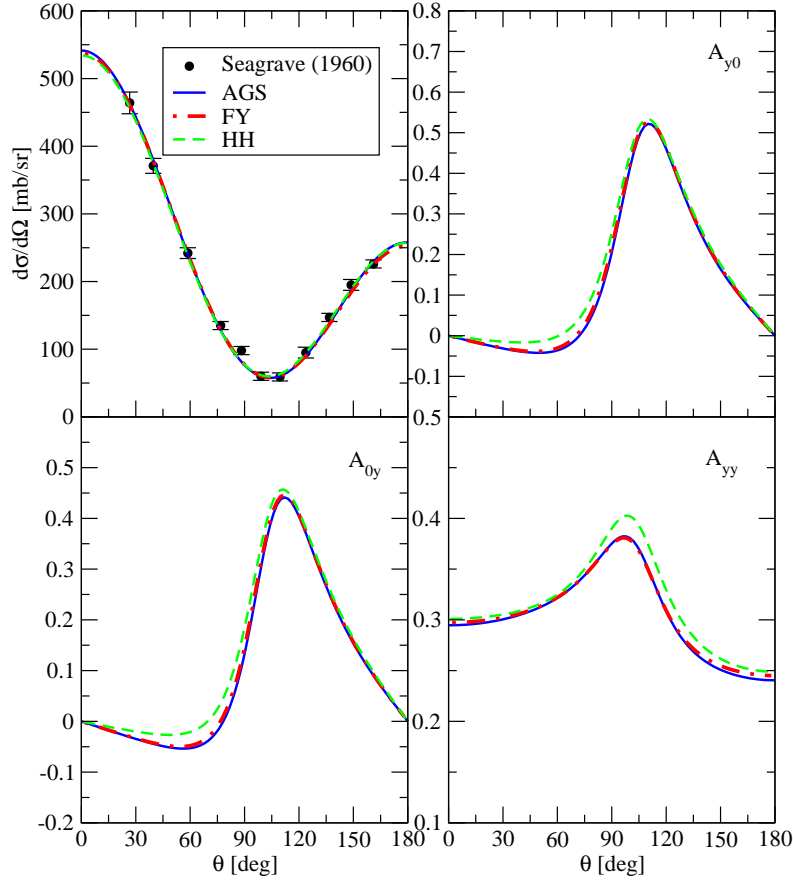


FIG. 4: (Color online) Same as Fig. 2 but for neutron energy  $E_n = 3.5$  MeV. The experimental data are from Ref. [42].

the analyzing power, and for the  $p\text{-}^3\text{H} \rightarrow n\text{-}^3\text{He}$  differential cross section at backward angles. These observables show also a sizable NN interaction model dependence [16]. Therefore as a paramount test of nuclear interaction models, it will be interesting to explore the effect of the inclusion of a 3N interaction. Work in this direction is in progress [70].

- 
- [1] S. Weinberg, Phys. Lett. B **251**, 288 (1990); Nucl. Phys. B **363**, 3 (1991); Phys. Lett. B **295**, 114 (1992)
  - [2] C. Ordonez, L. Ray, and U. van Kolck, Phys. Rev. C **53**, 2086 (1996)
  - [3] E. Epelbaum, H.W. Hammer, and U.-G. Meissner, Rev. Mod. Phys. **81**, 1773 (2009)
  - [4] R. Machleidt and D.R. Entem, Phys. Rep. **503**, 1 (2011)
  - [5] A. Deltuva, A. C. Fonseca, A. Kievsky, S. Rosati, P. U. Sauer, and M. Viviani, Phys. Rev. C **71**, 064003 (2005)
  - [6] H. Witala *et al.*, Phys. Rev. C **73**, 044004 (2006)
  - [7] H. Kamada *et al.*, Phys. Rev. C **64**, 044001 (2001)
  - [8] B. S. Pudliner, V. R. Pandharipande, J. Carlson, S. C. Pieper, and R. B. Wiringa, Phys. Rev. C **56**, 1720 (1997)
  - [9] R.B. Wiringa, S. C. Pieper, J. Carlson, and V. R. Pandharipande, Phys. Rev. C **62**, 014001 (2000)
  - [10] A. Nogga *et al.*, Phys. Rev. C **67**, 034004 (2003)
  - [11] R. Lazauskas and J. Carbonell, Phys. Rev. C **70**, 044002 (2004)
  - [12] M. Viviani, A. Kievsky, and S. Rosati, Phys. Rev. C **71**, 024006 (2005)
  - [13] P. Grassberger and W. Sandhas, Nucl. Phys. **B2**, 181 (1967); E. O. Alt, P. Grassberger, and W. Sandhas, JINR report No. E4-6688 (1972).
  - [14] A. Deltuva and A. C. Fonseca, Phys. Rev. C **75**, 014005 (2007)
  - [15] A. Deltuva and A. C. Fonseca, Phys. Rev. Lett. **98**, 162502 (2007)
  - [16] A. Deltuva and A. C. Fonseca, Phys. Rev. C **76**, 021001 (2007)
  - [17] E. O. Alt, W. Sandhas, and H. Ziegelmann, Phys. Rev. C **17**, 1981 (1978); *ibid.* **21**, 1733 (1980)

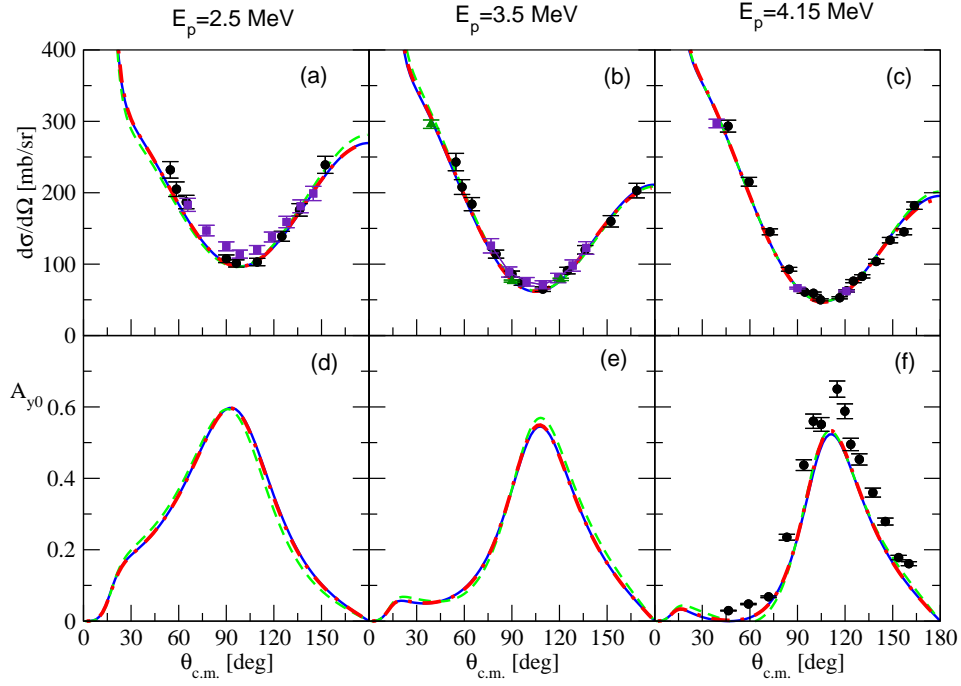


FIG. 5: (Color online) Differential cross sections (upper panels) and proton analyzing powers  $A_{y0}$  (lower panels) for  $p$ - $^3\text{H}$  elastic scattering at  $E_p = 2.5, 3.5,$  and  $4.15$  MeV proton energies obtained using the N3LO500 potential. The lines show the results obtained using the AGS (blue solid lines), FY (red dot-dash lines), and the HH (green dashed lines) methods. In many cases, the curves overlap and cannot be distinguished. The experimental data in panel (a) are from Refs. [36] (circles) and [35] (squares), in panel (b) from Refs. [36] (circles), [39] (squares), and [40] (triangles), in panel (c) from Refs. [41] (circles) and [40] (squares), and finally in panel (f) from Ref. [41] (circles).

- [18] A. Deltuva, A. C. Fonseca, and P.U. Sauer, Phys. Rev. C **71**, 054005 (2005); *ibid.*, **72**, 054004 (2005)
- [19] F. Ciesielski, *Thèse Univ. J. Fourier (Grenoble)* (1997); F. Ciesielski and J. Carbonell, Phys. Rev. C **58**, 58 (1998); F. Ciesielski, J. Carbonell, and C. Gignoux, Phys. Lett. **B447**, 199 (1999)
- [20] R. Lazauskas, *Thèse Univ. J. Fourier (Grenoble)* (2003)
- [21] R. Lazauskas, J. Carbonell, Nucl. Phys. A **737**, S79 (2004)
- [22] R. Lazauskas, J. Carbonell, A. C. Fonseca, M. Viviani, A. Kievsky, and S. Rosati, Phys. Rev. C **71**, 034004 (2005)
- [23] R. Lazauskas, Phys. Rev. C **79**, 054007 (2009)
- [24] A. Kievsky, S. Rosati, M. Viviani, L.E. Marcucci, and L. Girlanda, J. Phys. G: Nucl. Part. Phys. **35**, 063101 (2008)
- [25] M. Viviani, A. Kievsky, L. Girlanda, L. E. Marcucci, and S. Rosati, Few-Body Syst. **45**, 119 (2009)
- [26] M. Viviani, L. Girlanda, A. Kievsky, and L. E. Marcucci, Phys. Rev. Lett. **111**, 172302 (2013)
- [27] H. M. Hofmann and G. M. Hale, Nucl. Phys. **A613**, 69 (1997)
- [28] B. Pfitzinger, H. M. Hofmann, and G. M. Hale, Phys. Rev. C **64**, 044003 (2001)
- [29] H. M. Hofmann and G. M. Hale, Phys. Rev. C **68**, (2003) 021002; Phys. Rev. C **77**, 044002 (2008)
- [30] S. Quaglioni and P. Navrátil, Phys. Rev. Lett. **101**, 092501 (2008); Phys. Rev. C **79**, 044606 (2009)
- [31] P. Navrátil, S. Quaglioni, G. Hupin, C. Romero-Redondo, and A. Calci, Physica Scripta **91**, 053002 (2016)
- [32] M. Viviani *et al.*, Phys. Rev. C **84**, 054010 (2011)
- [33] A. Deltuva and A. C. Fonseca, Phys. Rev. Lett. **113**, 102502 (2014); Phys. Rev. C **90**, 044002 (2014)
- [34] D.R. Entem and R. Machleidt, Phys. Rev. C **68**, 041001 (2003)
- [35] A. Hemmendinger, G. A. Jarvis, and R. F. Taschek, Phys. Rev. **76**, 1137 (1949)
- [36] R.S. Claassen, R. J. S. Brown, G. D. Freier, and W. R. Stratton, Phys. Rev. **82**, 589 (1951)
- [37] N. Jarmie and R. C. Allen, Phys. Rev. **114**, 176 (1959)
- [38] J.E. Brolley Jr., T. M. Putnam, L. Rosen, and L. Stewart, Phys. Rev. **117**, 1307 (1960)
- [39] C. Manduchi, G. Moschini, G. Tornielli, and G. Zannoni, Nuovo Cim. **B57**, 340 (1968)
- [40] M. Ivanovich, P. G. Young, and G. G. Ohlsen, Nucl. Phys. **A110**, 441 (1968)
- [41] R. Kankowsky, J. C. Fritz, K. Kilian, A. Neufert, and D. Fick, Nucl. Phys. **A263**, 29 (1976)
- [42] J.D. Seagrave, L. Cranberg, and J. E. Simmons, Phys. Rev. **119**, 1981 (1960)
- [43] A.R. Sayres, K. W. Jones, and C. S. Wu, Phys. Rev. **122**, 1853 (1961)
- [44] V.P. Alfimenkov *et al.*, Yadernaya Fizika **33**, 891 (1981)
- [45] B. Haesner *et al.*, Phys. Rev. C **28**, 995 (1983)

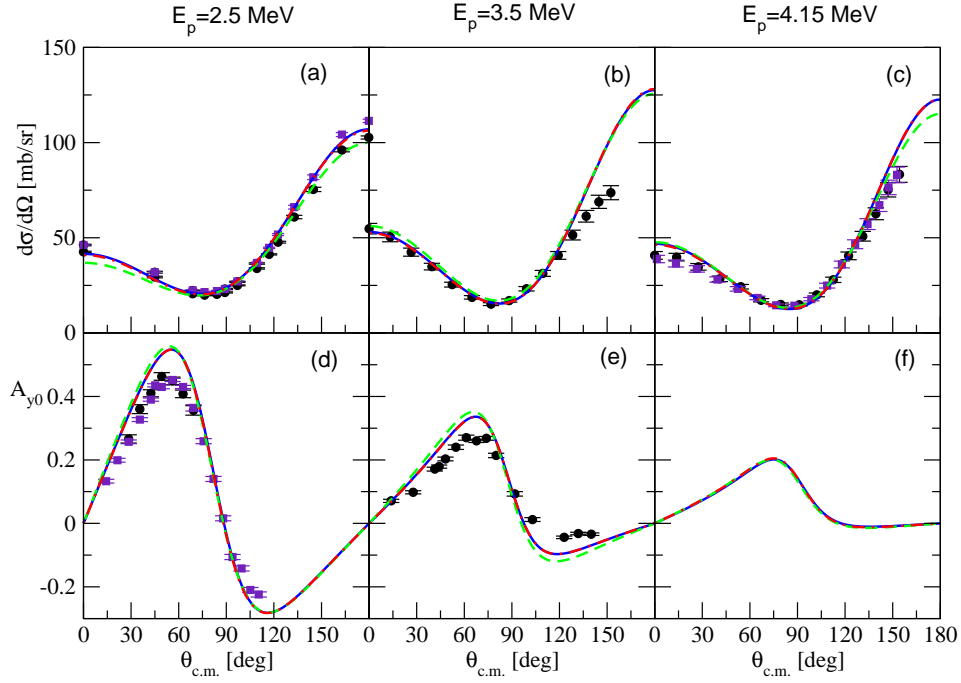


FIG. 6: (Color online) Same as Fig. 5 but for  $p\text{-}^3\text{H} \rightarrow n\text{-}^3\text{He}$  process. The experimental data in panel (a) are from Ref. [61] (circles), in panel (b) from Ref. [60] (circles), in panel (c) from Refs. [60] (circles) and [59] (squares), in panel (d) from Refs. [64] (circles) and [63] (squares), and finally in panel (e) from Ref. [63] (circles).

- [46] C.E. Hollandsworth, M. Gilpatrick, and W. P. Bucher, Phys. Rev. C **5**, 395 (1972)
- [47] K. Sinram, F. W. Buesser, and F. Niebergall, Proc. of the Int. Conf. on Interact. of Neutr. with Nuclei, Lowell, p. 1363, (1976)
- [48] H.O. Klages *et al.*, Nucl. Phys. **A443**, 237 (1985)
- [49] P. Jany, W. Heeringa, H.O. Klages, B. Zeitnitz, and R. Garrett Nucl. Phys. **A483**, 269 (1988)
- [50] J. Esterline, W. Tornow, A. Deltuva, and A. C. Fonseca, Phys. Rev. Lett. **110**, 152503 (2013)
- [51] J.H. Coon, Phys. Rev. **80**, 488 (1950)
- [52] R. Batchelor, R. Aves, and T. H. R. Skyrme, Rev. of Sci. Instruments **26**, 1037 (1955)
- [53] J.H. Gibbons and R. L. Macklin, Phys. Rev. **114**, 571 (1954)
- [54] J. Als-Nielsen and O. Dietrich, Phys. Rev. **133**, B925 (1964)
- [55] R.L. Macklin and J.H. Gibbons, Proc. of the Nuclear Structure Conf., Antwerp, p. 13 (1965)
- [56] D.G. Costello, S.J. Friesenhahn, and W.M. Lopez, Nucl. Sci. and Engineering **39**, 409 (1970)
- [57] S.B. Borzakov, K. Maletski, L.B. Pikelner, M. Stempinski, and E.I. Sharapov, Yadernaya Fizika **35**, 532 (1982)
- [58] G.A. Jarvis, A. Hemmendinger, H. V. Argo, and R. F. Taschek, Phys. Rev. **79**, 929 (1950)
- [59] H.B. Willard, J. K. Bair, and J. D. Kington, Phys. Rev. **90**, 865 (1953)
- [60] G.A. Jarvis, Los Alamos Scientific Report No. 2014, p. 35 (1956)
- [61] M. Drog, Los Alamos Scientific Report No. 8215 (1980)
- [62] D.S. Cramer and L. Cranberg, Nucl. Phys. **A171**, 59 (1971)
- [63] M.A. Doyle Sr., H.W. Clark, L.J. Dries, J.L. Regner, T.R. Donoghue, and G.M. Hale, Nucl. Phys. **A371**, 225 (1981)
- [64] W. Tornow, R.C. Byrd, P.W. Lisowski, R.L. Walter, and T.R. Donoghue, Nucl. Phys. **A371**, 235 (1981)
- [65] J.R. Walston *et al.*, Phys. Rev. C **58**, 1314 (1998)
- [66] W.S. Wilburn *et al.*, Few-Body Syst. **24**, 27 (1998)
- [67] M. Abramowitz and I. Stegun, *Handbook of Mathematical Functions* (Dover Publications, Inc., New York, 1970)
- [68] M. Viviani, Few-Body Syst. **25**, 177 (1998)
- [69] B. M. Fisher *et al.*, Phys. Rev. C **74**, 034001 (2006)
- [70] M. Viviani, L. Girlanda, A. Kievsky, and L. E. Marcucci, in preparation
- [71] L. D. Faddeev, Zh. Eksp. Teor. Fiz. **39**, 1459 (1960). [Sov. Phys. JETP **12**, 1014 (1961)]
- [72] O. A. Yakubovsky, Sov. J. Nucl. Phys. **5**, 937 (1967)
- [73] D. Baye, Phys. Rep. **565** (2015) 1